VICTORIA UNIVERSITY
MELBOURNE AUSTRALIA

Microglial activation induces nitric oxide signalling and alters protein S-nitrosylation patterns in extracellular vesicles

This is the Published version of the following publication

RESEARCH ARTICLE

Microglial activation induces nitric oxide signalling and alters protein S-nitrosylation patterns in extracellular vesicles

Natasha Vassileff[1] | Jereme G. Spiers[1,2,3] | Sarah E. Bamford[4] | Rohan G. T. Lowe[5] | Keshava K. Datta[5] | Paul J. Pigram[4] | Andrew F. Hill[1,6]

[1]The Department of Biochemistry and Chemistry, La Trobe Institute for Molecular Science, La Trobe University, Bundoora, Victoria, Australia

[2]Clear Vision Research, Eccles Institute of Neuroscience, John Curtin School of Medical Research, College of Health and Medicine, The Australian National University, Acton, Australia

[3]School of Medicine and Psychology, College of Health and Medicine, The Australian National University, Acton, Australia

[4]Centre for Materials and Surface Science and Department of Mathematical and Physical Sciences, La Trobe University, Bundoora, Victoria, Australia

[5]La Trobe University Proteomics and Metabolomics Platform, La Trobe University, Bundoora, Victoria, Australia

[6]Institute for Health and Sport, Victoria University, Melbourne, Australia

Correspondence
Andrew F. Hill, Institute for Health and Sport, Victoria University, Footscray, Melbourne, Australia. Email: andy.hill@vu.edu.au

Abstract

Neuroinflammation is an underlying feature of neurodegenerative conditions, often appearing early in the aetiology of a disease. Microglial activation, a prominent initiator of neuroinflammation, can be induced through lipopolysaccharide (LPS) treatment resulting in expression of the inducible form of nitric oxide synthase (iNOS), which produces nitric oxide (NO). NO post-translationally modifies cysteine thiols through S-nitrosylation, which can alter function of the target protein. Furthermore, packaging of these NO-modified proteins into extracellular vesicles (EVs) allows for the exertion of NO signalling in distant locations, resulting in further propagation of the neuroinflammatory phenotype. Despite this, the NO-modified proteome of activated microglial EVs has not been investigated. This study aimed to identify the protein post-translational modifications NO signalling induces in neuroinflammation. EVs isolated from LPS-treated microglia underwent mass spectral surface imaging using time of flight-secondary ion mass spectrometry (ToF-SIMS), in addition to iodolabelling and comparative proteomic analysis to identify post-translation S-nitrosylation modifications. ToF-SIMS imaging successfully identified cysteine thiol side chains modified through NO signalling in the LPS treated microglial-derived EV proteins. In addition, the iodolabelling proteomic analysis revealed that the EVs from LPS-treated microglia carried S-nitrosylated proteins indicative of neuroinflammation. These included known NO-modified proteins and those associated with LPS-induced microglial activation that may play an essential role in neuroinflammatory communication. Together, these results show activated microglia can exert broad NO signalling changes through the selective packaging of EVs during neuroinflammation.

KEYWORDS
extracellular vesicles, mass Spectral Imaging, Microglia, Neuroinflammation, Nitric Oxide, Nitrosylation, Post-translational modification, Proteomics, ToF-SIMS

Natasha Vassileff and Jereme G. Spiers contributed equally to this work.

- -

1 | INTRODUCTION

Neuroinflammation is a key change observed in several neurodegenerative diseases and often appears very early in disease pathogenesis (Bourgognon et al., 2021; Spiers et al., 2019). Whilst multiple signalling pathways and factors contribute to this change, microglial activation is one of the most important physiological determinates required for the initiation of neuroinflammation. Microglial cells exhibit a spectrum of activation profiles that can be classified based, in part, on their expression of inflammatory or anti-inflammatory markers (Bell-Temin et al., 2015). One of the principal markers used to characterise microglia as pro-inflammatory is the expression of the inducible form of nitric oxide synthase (iNOS) (Iizumi et al., 2016; Li et al., 2005). Under normal conditions, the expression of iNOS is extremely low, with the majority of nitric oxide (NO) produced in the brain being derived from the constitutively expressed and calcium-dependent neuronal or endothelial isoforms (Chen et al., 2019; Galea et al., 1992). However, activation of microglia induces iNOS expression, resulting in micromolar concentrations of NO production occurring in a calcium-independent manner. Released NO can signal via receptor interaction with soluble guanylyl cyclase or via two protein post-translational modifications (PTMs) which act to alter protein function, protein-protein interactions, or subcellular localisation (Nakamura & Lipton, 2019). Protein 3-nitrotyrosination (3-NT) is a relatively stable modification typically associated with NO damage due to the ability of this modification to facilitate protein aggregation in neurodegenerative diseases such as Alzheimer's disease (Wijasa et al., 2020). Protein S-nitrosylation is a much more labile interaction with NO attacking cysteine residues which can alter protein function via occupation of active sites and redox-active cysteines in addition to blocking subcellular signalling modifications requiring access to c-terminal cysteine residues (Nakamura & Lipton, 2019; Wijasa et al., 2020). Under neuroinflammatory conditions, increased NO availability from iNOS-derived NO production results in higher levels of NO-protein interaction facilitating PTM formation, ultimately changing a wide range of cellular functions and protein localisation.

As a signalling molecule, NO is diffusion limited and can react with target proteins or be sequestered by cellular antioxidants such as glutathione (Spiers et al., 2019). However, through protein PTMs, NO signalling can exert effects distant from the cellular site of NO production (Seth et al., 2019). This may be further extended outside the cell through the packaging of NO-modified proteins into extracellular vesicles (EVs) which afford a high degree of protein protection via encapsulation in a double lipid bilayer membrane (Todorova et al., 2017). Despite this, very few studies have investigated NO-modified proteins in EVs directly, instead focussing on EV biogenesis processes modulated by NO signalling (Chiaradia et al., 2021; Spiers et al., 2022). This is likely due to the difficulty in obtaining sufficient quantities of isolated EV proteins required to detect the fraction of NO-modifications within a sample. We have recently interrogated EVs using a surface-sensitive analytical technique, time of flight secondary ion mass spectrometry (ToF-SIMS), that can identify specific mass spectral signatures in surface preparations. In the present study, we have extended this work to demonstrate that ToF-SIMS can identify changes in NO-modifications of EVs released from activated microglia. We have further characterised the S-nitrosylated proteome of these EVs and identified key proteins associated with LPS-induced microglia activation that may play an essential role in neuroinflammatory communication.

2 | METHODS

2.1 | Microglial cell culture and LPS treatment

Mouse microglial (SIM-A9) cells were cultured in a 1:1 ratio of Dulbecco's Modified Eagle Medium (DMEM) (ThermoFisher Scientific 11965118): Ham's F-12 Nutrient Mix (ThermoFisher Scientific 11765062) containing 10% (v/v) foetal bovine serum (Sigma Aldrich F9423) and 5% (v/v) horse serum (ThermoFisher Scientific 16050122), the latter two of which were heat inactivated for 30 min at 50°C. Passaging involved collection of suspension cells and detachment of adherent cells using Dulbecco's Phosphate-Buffered Saline (DPBS) (ThermoFisher Scientific) containing 1 mM EDTA, 1 mM EGTA, and 1 mg/mL glucose. The cells were expanded in T175 flasks (ThermoFisher Scientific NUN159910) in 5% CO_2 at 37°C. Lipopolysaccharide (LPS) treatment consisted of culturing the SIM-A9 cells in a 1:1 ratio of DMEM (ThermoFisher Scientific 11965118): Ham's F-12 Nutrient Mix (ThermoFisher Scientific 11765062) containing 1% MEM Non-essential Amino Acid Solution (100×) (Sigma Aldrich M7145) and 1% glutamax (100X) (ThermoFisher Scientific 35050061) prior to addition of lipopolysaccharides from *Escherichia coli* (*E. coli*) O55:B5 (1 μg/mL; Sigma Aldrich L5418) and incubation in 5% CO_2 at 37°C for 48 h.

2.2 | Pro-inflammatory mRNA analysis

Cells seeded in 6-well plates were collected at 1.2×10^6 cells per sample for RNA isolation and mRNA analysis. RNA was extracted using the Qiagen miRNeasy mini kit (Qiagen 217004) according to the manufacturer's instructions. Reverse transcription of 1 μg of eluted RNA was achieved using a High-capacity cDNA Reverse Transcription kit (Applied Biosystems 4368813)

according to the manufacturer's instructions. Expression of mRNA was determined using 6-carboxyfluorescein-labelled Taqman Assay-on-demand kits for the following targets: Il1β (Mm00434228_M1), Il6 (Mm00446190_M1), Tnf (Mm00443258_M1), Ccl2 (Mm00441242_M1), Nfkbia (Mm00477798_m1), and Nos2 (Mm00440502_m1). Relative expression was calculated with the $\Delta\Delta$CT method using the geometric mean of Hprt1 (Mm03024075_m1), Actb (Mm02619580_g1), and Rpl13 (Mm02526700_g1) as housekeeping genes (Zhao et al., 2023).

2.3 | Nitric oxide (NO) metabolite assay

Measurement of the sample NO metabolites (nitrite and nitrate) concentration was achieved in the conditioned media using the nitrate/nitrite colorimetric assay kit (Cayman Chemical 780001) as per the manufacturer's instructions. Briefly, supernatant from cells seeded in 6-well plates at 1.2×10^6 cells per sample was collected for use in the assay. Enzyme Cofactor Mixture (Item No. 780012) and Nitrate Reductase Mixture (Item No. 780010) were added to the samples prior to incubation at room temperature for two hours. Griess Reagent R1 (Item No. 780018) and Griess Reagent R2 (Item No. 780020) were added to the samples prior to incubation at room temperature for 10 min and detection at 540 nm.

2.4 | Extracellular vesicle isolation

LPS-treated and untreated SIM-A9 cell culture supernatant was collected and centrifuged at $2000 \times g$ at 4°C for 10 min. The supernatant was transferred to 70 mL Polycarbonate tubes (Beckman Coulter) in a 45 Ti rotor (Beckman Coulter) and centrifuged at $10,000 \times g$ at 4°C for 30 min, the resulting supernatant was then centrifuged at $100,000 \times g$ at 4°C for 70 min. The generated pellet was then resuspended in 6 mL of DPBS and overlaid, in an Ultra-Clear thin wall 13.2 mL tube (Beckman Coulter), on a triple sucrose cushion composed of Fraction 4 (F4); 1 mL of 2.5 M sucrose, Fraction 3 (F3); 1.2 mL of 1.3 M sucrose, and Fraction 2 (F2); 1.2 mL of 0.6 M sucrose. The gradient was centrifuged at $200,000 \times g$ at 4°C for 180 min in a SW41 rotor (Beckman Coulter). The 1.2 mL fractions were then collected and resuspended in ice cold DPBS and centrifuged at $128,000 \times g$ at 4°C for 70 min in polycarbonate centrifuge bottles (Beckman Coulter) in a Type 70 Ti rotor (Beckman Coulter). The resulting pellets were resuspended in 100 μL of DPBS and stored at −30°C.

2.5 | Gel electrophoresis

Isolated vesicles and their parental cells were lysed in a solution containing 5 M NaCl, 1 M Tris, Triton X-100, 1% (w/v) sodium deoxycholate, and 1x cOmplete™ ULTRA protease inhibitor, at 4°C for 20 min prior to centrifugation at $2500 \times g$ for 5 min. Protein concentration of the resulting supernatant was resolved using the Pierce bicinchoninic acid (BCA) protein assay (ThermoFisher Scientific 23225) according to the manufacturer's instructions. LDS Sample Buffer (4X) (ThermoFisher Scientific NP0007) was then added to the supernatants prior to incubation for 10 min at 70°C. Samples were loaded onto a 4%–12% Bis-Tris Plus Gel (NuPAGE or Bolt; Invitrogen) for gel electrophoresis with 1X MES SDS running buffer (NuPAGE; Invitrogen). A PVDF membrane was used for protein transfer and was subsequently blocked in 5% skim milk in DPBS-T (0.05% Tween-20). The membranes were then probed with the following antibodies: Actin, Cell Signalling 8H10D10; Tsg101, Abcam ab30871; Flotillin-1, BD Bioscience 610821; Calnexin, Abcam ab22595; ApoB, Abcam ab139401, in 2.5% skim milk in DPBS-T. The probed membranes were then washed in DPBS-T and probed with either a mouse IgG HRP (BioStrategy NA931) or rabbit IgG HRP (BioStrategy NA934) secondary antibody. Clarity ECL reagent (Bio-Rad) was used for development of the membranes, which were then imaged with the ChemiDoc Touch imaging system (Bio-Rad) as per the manufacturer's recommendations and analysed using Image Lab 5.2.1 (Bio-Rad).

2.6 | Nanoparticle tracking analysis (NTA)

The size and concentration of the vesicles were determined using Nanoparticle Tracking Analysis (NTA) using the ZetaView© Quatt PMX-420 (Particle Metrix). The samples were diluted 1 in 1000 in filtered and degassed DPBS and loaded into a 1 mL syringe prior to injection into the instrument. The instrument recorded eleven positions, with each position capturing 30 frames using the following parameters: Maximum particle size: 1000, Minimum particle size: 10, Minimum Brightness: 25, Focus: autofocus, Sensitivity: 80.0, Shutter: 100, and Cell temperature: 25°C. The recordings were then analysed by the in-built ZetaView Software 8.05.14-SP7.

2.7 | Transmission electron microscopy (TEM) and scanning electron microscopy (SEM)

The size and morphology of the isolated vesicles were observed using transmission electron microscopy (TEM) and scanning electron microscopy (SEM). For TEM, 5 µL of the sample was blotted onto a formvar-copper coated grid (ProSciTech), previously glow discharge treated for 60 s. After 30 s the grid was blotted dry and Uranyl acetate (Agar Scientific) was applied for 10 s, twice. The grid was imaged using the JEM-2100 Transmission Electron Microscope (Jeol). For SEM, 1 µL of the sample was added to a 15 mm × 15 mm silicon wafer followed by 9 µL of DPBS. Samples were dried overnight and washed in increasing concentrations of ethanol in ultrapure water (50%, 70%, 90%, 95%, and 100%). Silicon wafers were then imaged using a Hitachi SU7000 field emission scanning electron microscope.

2.8 | Time of flight secondary ion mass spectrometry (ToF-SIMS) mass spectral imaging

Samples were prepared as described above for SEM with the silicon wafers being placed under vacuum in the IONTOF ToF-SIMS V instrument for mass spectral data acquisition as described previously (Bamford et al., 2023). Briefly, data were collected utilising a 30 keV Bi^{3+} primary ion source at one frame per patch and one shot per frame for 20 scans. In spectrometry mode (high mass resolution spectra), a 200 µm × 200 µm area was scanned in positive and negative ion mode, collecting 256 × 256 pixels, to a maximum of 1500 m/z and rastered in random mode. In fast-imaging mode (high spatial resolution images), 256 × 256 pixels were captured across a 20 × 20 µm area. As the primary ion dose (9×10^7 total dose) affected the delicate structure of the EVs, each spectrum was collected from a new area on the sample. Data were collected and analysed using the Surface Lab 7.2 data system. Co-localisation analysis was conducted using Image J software (Version 1.51j8), utilising the colocalization plugin (Bolte & CordeliÈRes, 2006).

2.9 | 3-Nitrotyrosine ELISA

Quantification of 3-nitrotyrosine levels was achieved using the 3-NT (3-Nitrotyrosine) ELISA Kit (Abcam ab116691) as per the manufacturer's instructions. Briefly, cells seeded in 6-well plates were collected at 1.2×10^6 cells per sample for protein extraction and use in the ELISA. Following addition of the standard or sample to each well, the plate was incubated for 2 h at room temperature. The wells were washed twice, and detector antibody was added to each well before incubation at room temperature for 1 h. The wells were washed twice again, and an HRP label was added to each well before incubation at room temperature for 1 h. The wells were washed three times again, and HRP Development Solution was added to each well prior to immediate reading at 600 nm for 15 min.

2.10 | Sample preparation for iodoTMT-based quantification of cysteine S-nitrosylated proteome

iodoTMT-labelled tryptic peptides were prepared as described previously (Wijasa et al., 2017) with some modifications. Briefly, EVs containing 100 µg of protein were resuspended in 100 µL of HENS lysis buffer (Thermo Scientific 90106), mixed, and disrupted in a sonicating water bath for 5 min before a short centrifugation. Methyl methanethiosulfonate (MMTS) (Pierce 23011) was used to block free thiols. MMTS was diluted to 120 mM using dimethyl formamide and 20 µL was added to each sample to obtain a final concentration of 20 mM. Samples were incubated in the dark for 30 min at room temperature on a shaker and protein precipitation was carried out by adding 480 µL of ice-cold acetone for an overnight incubation at −20°C.

The acetone pellet was resuspended in 50 µL HENS buffer. Nitrosyl groups were removed by adding 10 µL of sodium ascorbate (Sigma A7631) to each sample to achieve a final concentration of 20 mM. IodoTMT (Thermo Fisher Scientific 90103) labels resuspended in LC–MS grade methanol were immediately added to label the originally S-nitrosylated thiols. The control samples were labelled with 126, 127, and 128 while the LPS-treated samples were labelled with 129, 130, and 131 mass labels. The reaction mixtures were incubated at 37°C for 1 h in the dark.

Disulfide-bonded cysteines were reduced by addition of dithiothreitol to a final concentration of 20 mM and incubated for 15 min at 37°C. The six iodoTMT labelled samples were then pooled into one tube. The reduced disulfides were blocked by adding iodoacetamide to a final concentration of 15 mM and incubated for 10 min at 37°C in the dark. Protein precipitation was carried out by adding 2 mL of ice-cold acetone and incubation at −20°C for 4 h. The pellet was resuspended in 100 mM ammonium bicarbonate buffer (pH 8.0) and trypsin protease (Promega V5113) was added at a ratio of 1:50 (w/w). Digestion was carried out overnight at 37°C. The digestion was halted by the addition of trifluoroacetic acid to 0.5% (v/v). Labelled tryptic peptides were then desalted using C18 cartridges (Rappsilber et al., 2007) and dried in a rotary evaporator.

2.11 | Enrichment of iodoTMT containing peptides

Peptides were resuspended in 100 µL of Tris-buffered saline (TBS) (Pierce 28358). Anti-TMT resin (Thermo Fisher Scientific 90076) was washed three times with TBS and mixed with the peptides. Incubation was carried out for 4 h on a rotor at room temperature. The resin was washed three times in 100 µL TBS and three times in 100 µL water. Elution was carried out twice with TMT elution buffer (Thermo Fisher Scientific 90104). Eluted iodoTMT-labelled peptides were then dried and reconstituted in 8 µL of LC–MS loading buffer (2% (v/v) acetonitrile, 0.1% (v/v) trifluoroacetic acid).

2.12 | Sample preparation for label free quantification of total proteome

The single pot, solid phase, sample preparation strategy described previously (Hughes et al., 2019) was employed to prepare total proteome samples for mass spectrometry. Briefly, EVs containing 30 µg of protein were resuspended in 60 µL of HENS lysis buffer (Thermo Scientific 90106), mixed, and disrupted in a sonicating water bath for 5 min before a short centrifugation. Disulfide bonds were reduced by adding tris(2-carboxyethyl)phosphine to a final concentration of 5 mM and incubating at 60°C for 20 min. The reduced disulfide bonds were alkylated by adding iodoacetamide to a final concentration of 20 mM and incubating for 10 min in the dark at room temperature.

Proteins were captured onto carboxylate modified SpeedBeads (Cytiva 65152105050250 and 45152105050250) in a 50% ethanol mixture by incubating at 24°C for 5 min with shaking (900 rpm). The beads were separated using a magnetic rack, and the supernatant was discarded. The beads were washed 3 times with 80% ethanol, discarding the supernatant each time. Trypsin protease at a ratio of 1:20 (w/w enzyme:protein) was added in 20 mM ammonium bicarbonate and incubated at 37°C overnight on a shaker. The peptide solution was separated from the beads using a magnetic rack, and collected into fresh tubes. Samples were acidified by addition of trifluoroacetic acid to 0.5% (v/v). The tryptic peptides were then desalted using STAGE tips (Rappsilber et al., 2007) and dried in a rotary evaporator.

2.13 | LC–MS/MS analysis of peptides

The mass spectrometry acquisition methods for both total proteome and iodoTMT-labelled peptides were identical. LC–MS was performed on a Thermo Ultimate 3000 RSLCnano UHPLC system and a Thermo Q-Exactive HF mass spectrometer. Peptides were reconstituted in 0.1% (v/v) trifluoroacetic acid (TFA) and 2% (v/v) acetonitrile (ACN). Peptides were loaded onto a PepMap C18 5 µm 1 cm trapping cartridge (Thermo-Fisher Scientific, Waltham, MA, USA) at 14 µL/min and washed for 6 min before switching the pre-column in line with the analytical column (nanoEase M/Z Peptide BEH C18 Column, 1.7 µm, 130 Å and 75 µm ID × 25 cm, Waters). The separation of peptides was performed at 250 nL/min using a linear ACN gradient of buffer A (0.1% (v/v) formic acid, 2% (v/v) ACN) and buffer B (0.1% (v/v) formic acid, 80% (v/v) ACN), starting at 5% buffer B to 50% over 84 min, then rising to 80% B over 15 min followed by 95% B for 5 min. The column was then cleaned for 5 min at 95% B, ramped down to 2% B in 2 min, with a final 3 min equilibration step at 2% B. The total runtime was 120 min. Blanks were run between samples with a full column equilibration step before the next sample injection.

Data were collected on a Thermo Q-Exactive HF Orbitrap (Thermo-Fisher Scientific, Waltham, MA, USA) in Data Dependent Acquisition mode using m/z 350−1500 as MS scan range and HCD MS/MS spectra were collected in the Orbitrap using topN = 7 cycle loop. Dynamic exclusion parameters were set with 'exclude isotope' on and a duration of 25 s. Other parameters for the instrument were: MS1 scan at 60,000 resolution, injection time 30 ms, AGC target 3e6, HCD collision energy 28%, injection time Auto with AGC target at Standard. MS2 scan was at 30,000 resolution, 200–2000 m/z scan range, AGC of 1e5 and max IT of 110 ms. The isolation window of the quadrupole for the precursor was 1.4 m/z. An internal lock mass of 445.12003 m/z was used.

2.14 | LC–MS/MS data processing

Raw files obtained from mass spectrometry analysis were searched against the UniProt mouse protein database using Sequest HT through Proteome Discoverer (Version 2.4) (Thermo Scientific, Bremen, Germany). Precursor and fragment mass tolerance were set to 20 ppm and 0.05 Da, respectively. For total proteome data, carbamidomethylation of cysteine was set as fixed modification while oxidation of methionine and deamidation of asparagine and glutamine were set as dynamic modifications. For iodoTMT data, carbamidomethylation of cysteine, iodoTMT at cysteine were set as dynamic modifications in addition to oxidation of methionine and deamidation of asparagine and glutamine. Acetylation at protein N-terminus was set as a dynamic modification for both datasets. A false discovery rate (FDR) threshold of 1% was used to filter peptide spectrum matches (PSMs). FDR was calculated using a decoy search. For iodoTMT data, an iodoTMT localization probability was calculated using the ptmRS node.
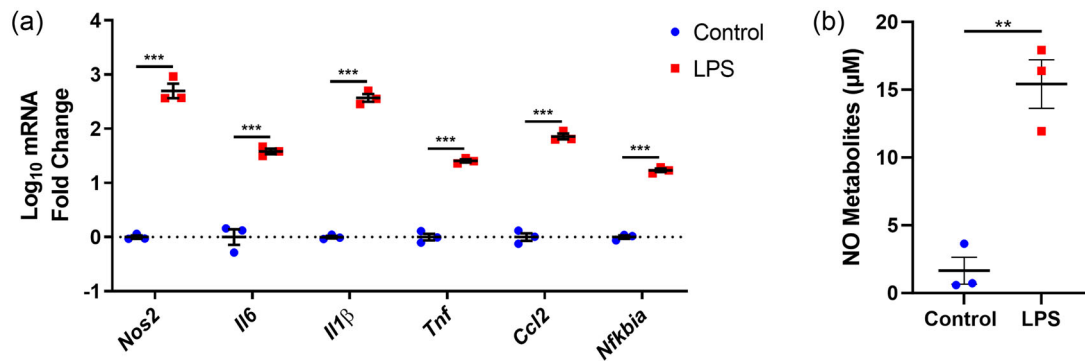
FIGURE 1   Characterisation of the LPS treatment performed on SIM-A9 microglial cells. 1 μg/μL of lipopolysaccharide (LPS) treatment elicited a strong inflammatory response in treated microglial cells. (a) Cells treated with LPS exhibited a significant increase in their gene expression of cytokines: Il6, Il1β, Tnf, and Ccl2, in addition to Nfkbia and the inducible form of nitric oxide synthase (Nos2) compared to untreated control cells. (b) NO metabolites (nitrate and nitrite) levels were also found to be significantly increased in cells treated with LPS compared to controls, confirming the presence of a neuroinflammatory phenotype. Data was compared using unpaired *t*-test and expressed as mean ± SEM, *$p < 0.05$.

2.15 | Statistical analysis and data availability

Data for pro-inflammatory mRNA expression, nitrate/nitrite metabolites, and 3-nitrotyrosine protein modifications were analysed using GraphPad Prism (Version 8.2.1; GraphPad Software Inc, San Diego, CA, USA). Control and LPS-treated groups were all compared using individual Student's *t*-tests. All data were presented as the mean ± standard error of the mean (SEM) and $p < 0.05$ was considered statistically significant. Differential analysis was conducted using the limma package based on protein-wise linear models and empirical Bayes statistics. The adjusted *p*-value was set at <0.05 and the fold change was set to >1.5 or <−1.5. The resulting data was presented using GraphPad Prism (Version 8.2.1; GraphPad Software Inc, San Diego, CA, USA). Further downstream analysis was conducted using STRING analysis and FunRich 3.1.3, the results from which were presented using Microsoft Excel (Fonseka et al., 2021; Szklarczyk et al., 2015).

The proteomics data has been submitted to the PRIDE repository and can be accessed using the identifier PXD044914.

3 | RESULTS

3.1 | LPS induces iNOS expression in treated microglial cells

The treatment of microglial cells with LPS elicited a clear inflammatory response as evidenced by the increase in cytokines: Interleukin 6 (Il6; $p < 0.001$), Interleukin 1β (Il1β; $p < 0.001$), tumour necrosis factor (Tnf; $p < 0.001$), C-C motif chemokine 2 (Ccl2; $p < 0.001$), and the inflammatory indicator nuclear factor of kappa light polypeptide gene enhancer in B-cells inhibitor alpha (Nfkbia; $p < 0.001$) (Figure 1a). In addition, the treated cells demonstrated a significant decrease in the expression of two redox regulators; nuclear factor erythroid 2-related factor 2 (Nfe2l2; $p < 0.01$) and glutamate-cysteine ligase catalytic subunit (Gclc; $p < 0.05$), the latter of whose expression is known to decrease in an inflammatory response due to mRNA decay and caspase-5 mediated protein degradation (Figure S1) (Zhang et al., 2020). Increased gene expression of the inducible form of NO synthase (Nos2; $p < 0.001$) was also observed in the treated cells, characteristic of classically activated microglia (Figure 1a). This alluded to an increase in NO production which was confirmed by the increased NO metabolite levels ($p < 0.01$) detected in the LPS treated cells (Figure 1b), verifying the LPS elicited a neuroinflammatory phenotype (Kumar et al., 2014; Li et al., 2005).

3.2 | EVs were successfully isolated from LPS treated microglial cells

Following confirmation of a neuroinflammatory response, the EV content released from treated microglia was analysed to determine whether NO modified proteins were being packaged in EVs. However, firstly the secreted vesicles were characterised to confirm they met the minimum criteria required by the International Society of Extracellular Vesicles 2018 (MISEV2018) to be classified as small EVs (Théry et al., 2018). The isolated vesicles were found to exhibit a presence of characteristic small EV markers and an absence of small EV non-enriched markers (Figure 2a). The 100–150 nm diameter of the EVs and their depressed cup like structure further demonstrated their morphological resemblance to small EVs, allowing them to meet the MISEV2018 guidelines (Figure 2b and c) (Théry et al., 2018). In addition to TEM, the EVs underwent SEM on a silica wafer to ensure they
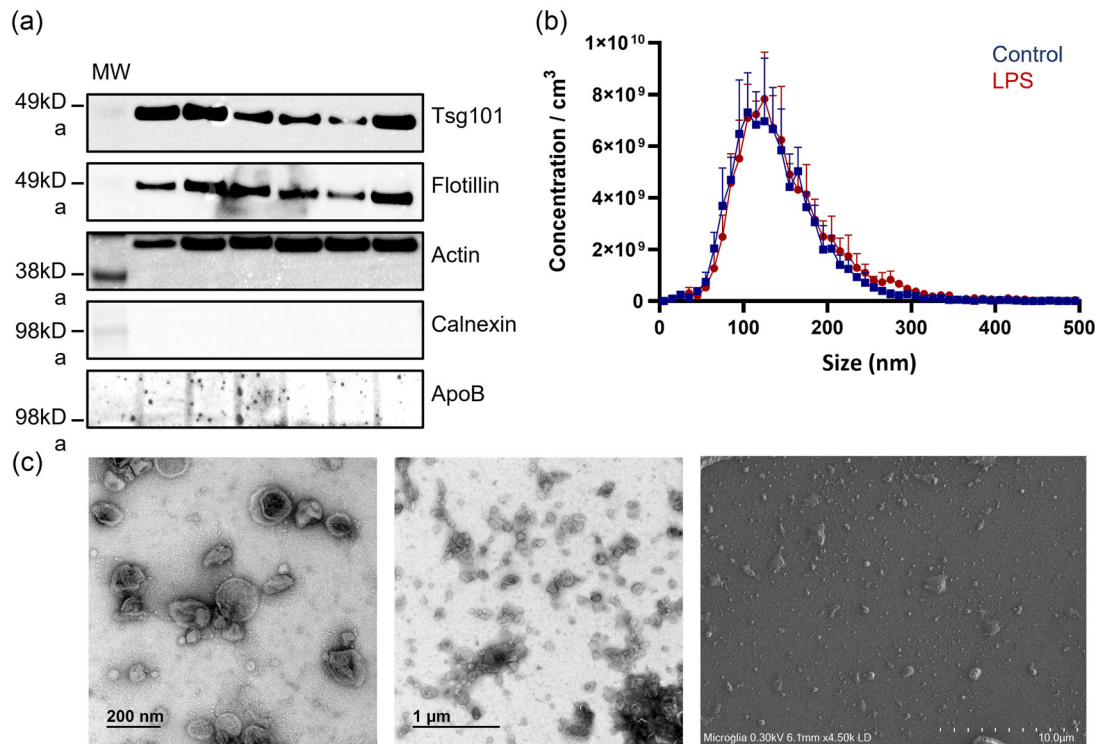
FIGURE 2 Characterisation of extracellular vesicles (EVs) from microglia. EVs isolated from microglial cells with/without LPS treatment appear to exhibit characteristics consistent with that of small EVs. (a) The isolated vesicles were positive for small EV enriched markers tsg101, flotillin, and actin, and negative for small EV non-enriched markers; calnexin and ApoB. (b) Nanoparticle tracking analysis, performed on the ZetaView© Quatt PMX-420, demonstrates the vesicles appear to be between 100 and 150 nm in diameter, consistent with small EVs. This result is representative of $n = 6$. (c) Transmission electron microscopy (TEM) and scanning electron microscopy (SEM) images exhibit a population of vesicles with depressed cup-like structures and a diameter of 100–200 nm, consistent with that of small EVs. These images are of a representative sample.

maintained their structural integrity during the surface preparation process required for ToF-SIMS, a technique that we have recently used to elucidate broad biochemical changes (Figure 2c) (Bamford et al., 2023).

3.3 | EVs from LPS treated microglial cells exhibited biochemical changes consistent with NO-induced modifications

Physiological changes in the EVs from LPS-treated microglia were observed using ToF-SIMS. Imaging data was extracted for nitrite (NO_2^-) and nitrotyrosine ($C_6H_4NO_3^-$) using Fast-Imaging mode to determine whether proteins post-translationally modified by peroxynitrite were packaged into EVs (Figure 3a). Following pseudo-colouring and correlation analysis, a moderate degree of overlap in NO_2^- and nitrotyrosine was observed, indicative of NO-modified proteins. Additionally, the NO_2^- peak collected in Spectrometry mode correlated with the increased 3-nitrotyrosine levels ($p < 0.05$) detected by ELISA in the EVs from LPS-treated cells compared to controls (Figure 3b). In addition to nitrotyrosine, imaging data for Cysteine ($C_3H_7SNO_2^-$) and sulphur-bound hydrogen thiol (HS^-) was extracted and overlayed with NO_2^- (Figure 3a). Cysteine and sulphur-bound hydrogen thiol are known to be oxidised by NO and peroxynitrite under inflammatory conditions. Using colocalization analysis, a much higher degree of overlap was observed between NO_2^- and both cysteine and sulphur-bound hydrogen thiol, indicating the functional side chain of cysteine was being modified by NO and packaged into EVs under inflammatory conditions. Therefore, iodolabelling and total proteome analysis was performed to identify which proteins were undergoing this modification and being packaged into EVs.

3.4 | Differentially S-nitrosylated proteins were identified in the EVs from LPS treated microglial cells

Total proteome analysis was initially performed to normalise the iodolabelling results and bring context to the changes observed, in addition to further confirm the neuroinflammatory LPS model (Figure 4a). Through total proteome analysis, 15 significantly
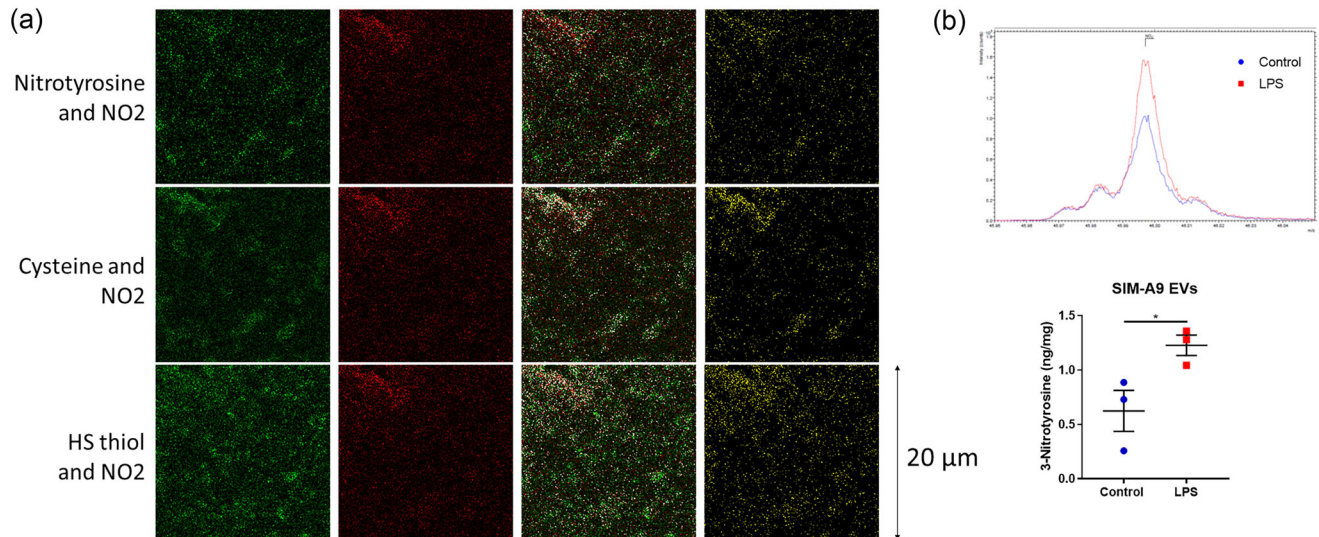
(a)

(b)

20 μm

FIGURE 3 Physiological target analysis from ToF-SIMS imaging data. (a) Nitrotyrosine($C_6H_4NO_3{}^-$), Cysteine ($C_3H_7SNO_2{}^-$) and sulphur-bound hydrogen thiol (HS^-) imaging data were pseudo-coloured green. Each image was overlaid with $NO_2{}^-$ (red), and colocalised pixels were recoloured white. After background removal co-located pixels were re-coloured yellow. All mass spectral images were captured using Fast–Imaging mode. Each image has a 20 μm × 20 μm field of view. (b) The NO_2 peak collected in Spectrometry mode correlated with the 3-nitrotyrosine levels which were found to be significantly elevated in EVs isolated from LPS-treated microglial cells compared to controls. Data were compared using unpaired t-test and expressed as mean ± SEM, $^*p < 0.05$.

differentially expressed proteins were identified in the LPS-treated microglial EVs compared to the controls. These included the pro-inflammatory cytokines; Tnf and C-X-C motif chemokine ligand 10 (cxcl10), and superoxide dismutase 2 (Sod2), a mitochondrial superoxide dismutase, which is known to be up-regulated following LPS treatment (Real et al., 2018). Following analysis of the total proteome, iodolabelling was performed on the EVs to identify changes in EV protein S-nitrosylation when compared to changes in the total EV proteome. These widespread changes, highlighted in Figure 4b, can be broadly divided into proteins with increased S-nitrosylation relative to the total proteome (depicted in red in Figure 4b) and those with decreased S-nitrosylation relative to the total proteome (depicted in blue in Figure 4b). Proteins belonging to the former group included the 26S proteasomal subunit at C170 on 10B and C210 on 6B, which is involved in proteasomal clearance, and Cathepsin B at C93, a lysosomal cysteine protease involved in intracellular proteolysis. Conversely, the following proteins were found to have an increased total proteome expression but comparatively decreased S-nitrosylation in the EVs from LPS-treated cells; pyruvate kinase (PKM) at C152, Macrosialin at C283, and cluster of differentiation 14 (CD14) at C213. Interestingly, several proteins including actin-β chain at C285 and Nicotinamide phosphoribosyltransferase (NAMPT) at C39 were found to exhibit both increased S-nitrosylation and increased protein expression in EVs isolated from treated cells (Figure S2A). Overall, 121 proteins were found have at least one cysteine residue S-nitrosylated due to NO, highlighting the vast influence this cellular regulator has under neuroinflammatory conditions (Figure S2B). The S-nitrosylated EV proteome was further examined through Gene Ontology (GO) analysis to identify pathways impacted by neuroinflammatory NO signalling.

3.5 | EV proteins from LPS treated microglial cells were found to be involved in key immunomodulatory pathways

The pathway effects of these S-nitrosylation changes were investigated via gene ontology (GO) analysis (Figure 5a). Complement component receptor activity and interleukin receptor binding were determined to be molecular functions of the proteins exhibiting significant EV protein S-nitrosylation changes when compared to changes in the total EV proteome. The proteins were also found to function in proteolysis and be involved in the transfer of LPS to CD14 and TLR4 cascades. GO analysis of proteins with S-nitrosylation changes consistent with their total proteome expression yielded similar results (Figure S3A). These included the molecular functions; complement and interleukin receptor activity, cellular component locations; NF-κB complexes, and reactome pathways involving the inflammatory response. STRING analysis showed the majority of proteins with significant changes in EV protein S-nitrosylation when compared to changes in the total EV proteome or those with S-nitrosylation changes consistent with their total proteome expression were known interacting partners and exhibited network relationships (Figures 5b and S3B). However, this phenomenon was not observed for proteins significantly differentially expressed when examining the total
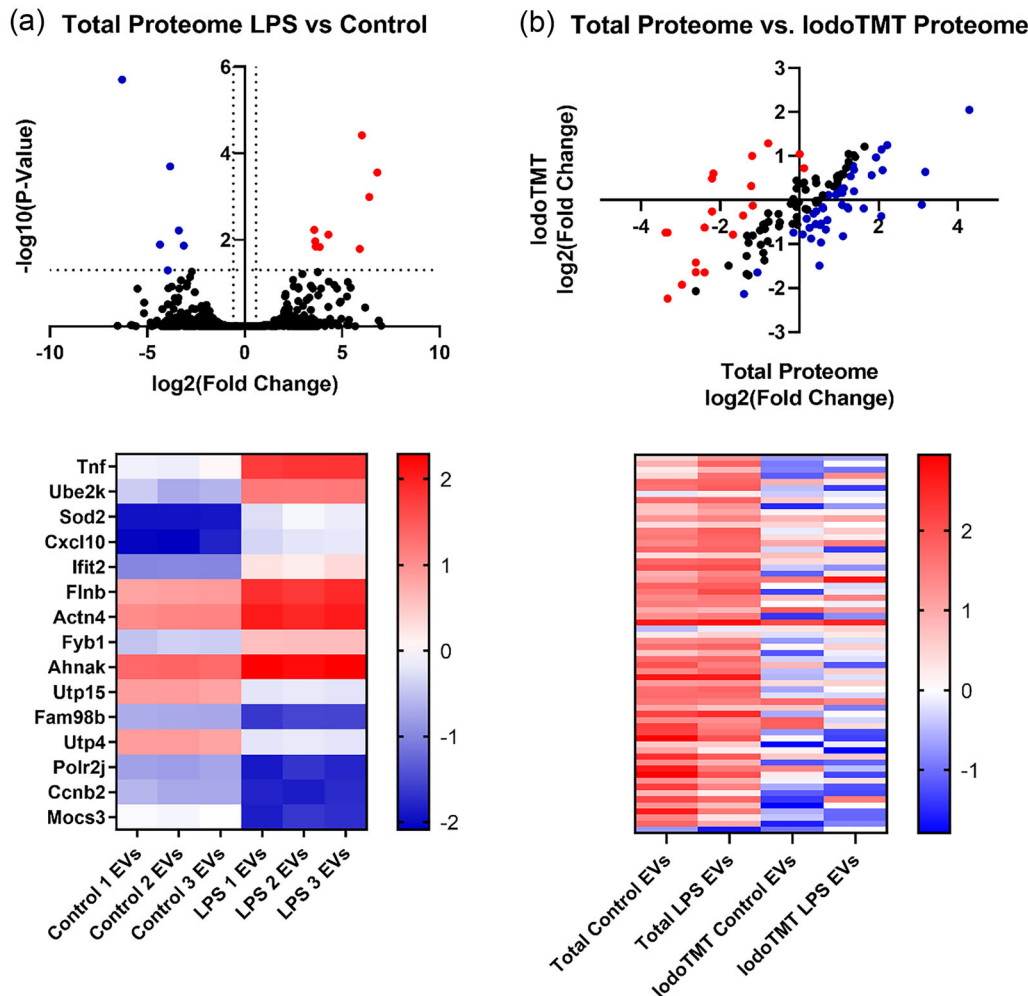
FIGURE 4 Significant proteins in the total proteome and those with altered S-nitrosylation in the LPS treated microglial EVs compared to controls. (a) Fifteen proteins were found to be significantly differentially expressed in the LPS treated microglial EVs compared to the control microglial EVs with many being key players in the inflammatory response. (b) The detection of proteins with altered S-ntirosylation encompasses those with either increased or decreased S-ntirosylation when compared to their total proteome.

proteome alone (Figure S3C). Therefore, the S-nitrosylation changes occurring in the context of the total proteome expression appear to be interconnected and selectively packaged into EVs during neuroinflammation.

4 | DISCUSSION

Microglial expression of inducible NO synthase and subsequent NO production contributed to key changes in protein S-nitrosylation patterns indicative of neuroinflammation. However, to our knowledge, this is the first study to investigate the S-nitrosylated proteome in EVs following an inflammatory stimulus. Using a novel imaging method, we have shown that EVs released from LPS-stimulated microglia exhibit observable increases in NO signalling that are localised with protein cysteine thiol side chains. Proteomic analysis revealed significant alterations in EV protein nitrosylation patterns relative to changes in the total EV proteome, with a large proportion of NO-modified proteins being functionally involved in innate immunity. This shows activation of microglia results in broad signalling changes extending beyond the diffusion-limited spatial domains of NOS-produced NO.

During inflammation, gene expression of the inducible form of NO synthase (Nos2) leads to translation of the iNOS protein which generates large amounts of NO. This phenomenon, characteristic of classically activated microglia, was observed in the treated cells, alluding to an increase in NO production which was confirmed by the increased NO metabolite levels (Figure 1b) verifying LPS elicited a neuroinflammatory phenotype (Kumar et al., 2014; Li et al., 2005). The produced NO can then be oxidised to peroxynitrite in the presence of hydrogen peroxide and superoxide radicals producing an oxidant that leads to the

(a)

Molecular Function

- complement component C3b receptor activity
- complement component C4b receptor activity
- opsonin binding
- thymidylate kinase activity
- eukaryotic initiation factor 4G binding
- interleukin-1 type I receptor antagonist activity
- interleukin-1 type II receptor antagonist activity
- interleukin-1, type II receptor binding
- inositol-3-phosphate synthase activity
- protein histidine kinase activity

Cellular Component

- integrin alphaM-beta2 complex
- basal ectoplasmic specialization
- cofilin-actin rod
- pyruvate kinase complex
- cytoskeletal calyx
- membrane microdomain
- IRE1-RACK1-PP2A complex
- integrin alpha5-beta1 complex
- integrin alphaL-beta2 complex
- phenylalanine-tRNA ligase complex

Biological Function

- regulation of blood coagulation, intrinsic pathway
- constitutive protein ectodomain proteolysis
- negative regulation of bleb assembly
- dTDP biosynthetic process
- negative regulation of postsynaptic density organization
- negative regulation of unidimensional cell growth
- positive regulation of establishment of cell polarity
- positive regulation of protein localization
- positive regulation of prostaglandin-E synthase activity
- positive regulation of erythrocyte aggregation

Protein Domain

- CLH
- UBA_e1_C
- FIMAC
- AdoHcyase
- AdoHcyase_NAD
- Enolase_N
- Enolase_C
- Integrin_b_cyt
- Int_alpha
- Integrin_B_tail

Reactome Pathway

- Transfer of LPS from LBP carrier to CD14
- Association of TriC/CCT with target proteins during biosynthesis
- MyD88-independent TLR4 cascade
- Toll Like Receptor 4 (TLR4) Cascade
- Fibronectin matrix formation
- Galactose catabolism
- Caspase activation via Death Receptors in the presence of ligand
- TRIF-mediated programmed cell death
- ARMS-mediated activation
- RHO GTPases Activate ROCKs

(b)

FIGURE 5 Gene ontology (GO) analysis and search tool for the retrieval of interacting genes/proteins (STRING) analysis of proteins with altered S-nitrosylation in the LPS treated microglial EVs compared to controls. (a) GO analysis based on fold enrichment revealed the proteins exhibit molecular functions including complement and interleukin receptor activity; cellular component locations including integrin complexes; biological processes including regulation of post-synaptic density; protein domains including enolase and integrins; and reactome analysis uncovered the proteins to be involved in the inflammatory responses including those associated with LPS. (b) The majority of proteins with either increased or decreased S-nitrosylation when compared to their total proteome, in the treated microglial EVs, appear to exhibit network relationships/connectivity. The graph was created using STRING.

post-translational modification of proteins (Kumar et al., 2014). Physiological changes relating to these post-translational modifications were observed in the EVs from LPS-treated microglia using ToF-SIMS and a 3-nitrotyrosine ELISA. This demonstrated that nitrotyrosine-containing proteins were being packaged into EVs and may represent a mode of communication between cells during neuroinflammation. Importantly, the large overlap between NO_2^- and both cysteine and sulphur-bound hydrogen thiols indicated modification of cysteine's functional side chain by NO and subsequent packaging into EVs under inflammatory conditions. Although the ToF-SIMS results demonstrated packaging of NO-modified proteins into EVs, another technique, iodolabelling, was required to identify these S-nitrosylated proteins.

Prior to iodolabelling, total proteome analysis was performed on each sample. This further confirmed the neuroinflammatory LPS model and was vital for normalisation of the iodolabelling results. The total proteomic analysis of the microglial cell derived EVs revealed differential expression of pro-inflammatory cytokines Tnf and cxcl10, which are known to be produced in response to LPS and have previously been found to be enriched in microglial EVs and immune cell derived EVs upon inflammation (Javeed et al., 2021; Yaker et al., 2022; Yang et al., 2018). In addition, Sod2, a mitochondrial superoxide dismutase known to convert superoxide into the less toxic hydrogen peroxide and oxygen by-products, was found to be enriched in the LPS-treated microglial EVs. Sod2 is known to be up-regulated following LPS treatment and has previously been detected in plasma EVs isolated from sepsis patients, a condition for which LPS is one of the most potent microbial mediators (Prebanda et al., 2019; Real et al., 2018). Following analysis of the total proteome, iodolabelling was performed on the EVs.

The iodolabelling revealed significant changes in EV protein S-nitrosylation when compared to changes in the total EV proteome (Figure 6). These changes included the S-nitrosylation of Cathepsin B by NO at C93, which inhibits its activity leading to impeded autophagy initiation, protein aggregate accumulation, and increased autolysosomal vesicle generation culminating in a blockade of autophagic flux (Kim et al., 2022). Under these conditions, autolysosomal vesicles are known to fuse with multivesicular bodies and exchange material that can be packaged into intraluminal vesicles resulting in EV release (Eitan et al., 2016; Mizushima, 2007; Murrow et al., 2015). In addition to Cathepsin B, the 26S proteosomal regulatory subunit exhibited increased S-nitrosylation, at C170 on 10B and C210 on 6B, relative to its total proteome. Both the catalytic region and the regulatory region of the 26S proteosome have been shown to be S-nitrosylated with these modifications inhibiting the proteosome and its ability to degrade proteins (Kapadia et al., 2009; Murray et al., 2012). Specifically, the 20S proteasome, proteasome activator PA28, and 19S proteasome regulator have been discovered inside microvesicles released by activated T lymphocytes (Bochmann et al., 2014). This selective packaging is believed to assist in the generation of extracellular proteasomes, characteristically found in vivo in sufferers of inflammatory diseases (Bochmann et al., 2014). Interestingly, in our study GO analysis revealed proteolysis to be a function heavily involving these differentially nitrosylated proteins. Conversely, EV proteins exhibiting decreased nitrosylation relative to their total proteome expression included PKM, macrosialin, CD14, and integrin subunit α5 (ITGA5). S-nitrosylation of PKM in the presence of NO has been found to divert glucose metabolic flux from glycolysis into the pentose phosphate pathway to increase production of reducing molecules (Yang et al., 2022). Therefore, lower PKM S-nitrosylation promotes glycolysis and favours oxidative stress. It has been shown that EVs enriched in PKM2 are capable of promoting macrophage activation and therefore the packaging of this enzyme into EVs may be an attempt to promote the inflammatory response (Tan et al., 2022). Macrosialin, a macrophage infiltration marker and CD14 a monocyte differentiation antigen, are known to exhibit increased expression upon LPS stimulation (Futami et al., 2022; Hassani & Olivier, 2013; Mahida et al., 2022; Papageorgiou et al., 2016). These proteins have also been found to be significantly enriched in EVs from patients suffering from sepsis and other inflammatory conditions (Futami et al., 2022; Hassani & Olivier, 2013; Mahida et al., 2022; Papageorgiou et al., 2016). Therefore, the decreased S-nitrosylation of macrosialin and CD14 coupled with their EV packaging may be intended to activate neighbouring macrophages. Alternatively, given the increased total proteome expression of these proteins, the S-nitrosylation may not be functionally regulating these proteins relative to their expression following LPS treatment. Finally, the enrichment of ITGA5 with comparatively decreased S-nitrosylation in the EVs from LPS treated cells was consistent with its increased expression in patients suffering from inflammatory conditions (Xu et al., 2021). This result is consistent with the detection of interleukin receptor activity through GO analysis of the differentially S-nitrosylated EV proteome. Furthermore, identification of complement component activity in the EVs is consistent with the expression of complement regulators on the surface of EVs under inflammatory conditions, leaving recipient cells or pathogens vulnerable to complement attacks (Ebrahimi et al., 2013). The GO terms; cytoskeletal calyx and membrane microdomain, may further be related to the cytoskeletal remodelling involving ITGA5 (Xu et al., 2021). Finally, enrichment of ITGA5 has been linked to actin organisation during immune cell activation (Xu et al., 2021). Macrophage actin cytoskeleton remodelling for cellular contraction and spreading has been documented to occur in response to LPS stimulation (Ronzier et al., 2022). Furthermore, S-nitrosylation of actin has been documented in vivo and in vitro under inflammatory conditions (Lu et al., 2011). In accordance with the literature, upregulation of actin-β chain expression and S-nitrosylation, at C285, was observed in this study along with several other proteins known to be involved in complement and interleukin receptor activity and NF-κB complexes, consistent with an immune response as supported by the reactome results. These proteins were found to be involved in biological processes including regulation of cell polarity and protein localization to the leading edge, which may be attributed to the role actin plays in activating macrophages (Ronzier et al., 2022). Additionally, NAMPT was found to exhibit increased S-nitrosylation, at C39, consistent with its total proteome expression. NAMPT is known to function as an immunomodulatory cytokine extracellularly and is a promising biomarker for sepsis (Karampela et al., 2019). Further-
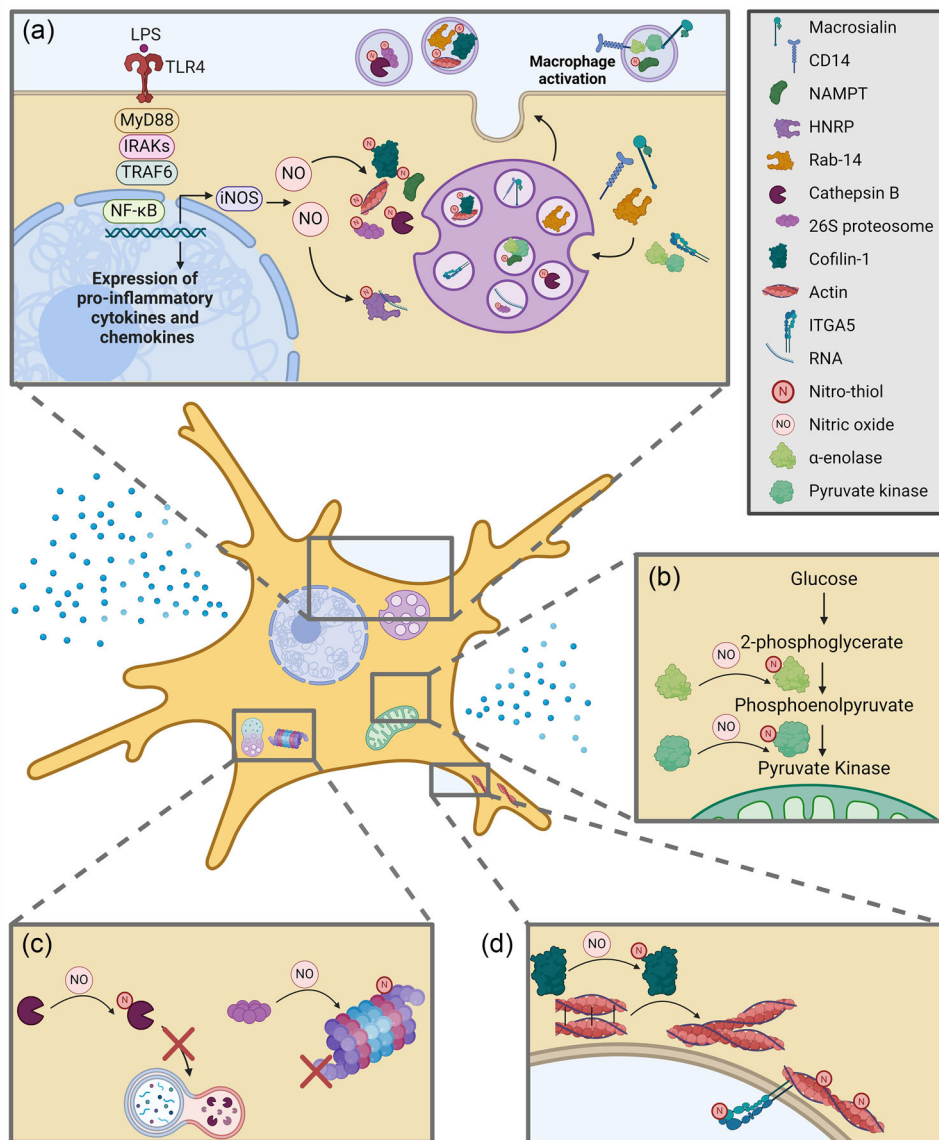
FIGURE 6 Neuroinflammatory signalling alters microglia through S-nitrosylation which is represented in their released extracellular vesicles (EVs). A (*Left*) Lipopolysaccharide (LPS) binds to Toll like receptor 4 (TLR4) leading to a cascade of signals culminating in nuclear factor kappa-light-chain-enhancer of activated B cells (NF-κB) activation and expression of pro-inflammatory cytokines and chemokines in addition to inducible nitric oxide synthase (iNOS) which generates nitric oxide (NO), a molecule that leads to nitrothiol modifications on proteins in a process known as S-nitrosylation. These modified proteins (*Right*) are then packaged into EVs which when taken up by recipient cells are capable of potentiating the neuroinflammatory signal. B Upon LPS stimulation, both glycolytic proteins; α-enolase and pyruvate kinase are nitrosylated leading to altered glycolysis in the microglia, a process that is required for microglia to maintain their activated state. These proteins undergo increased nitrosylation in the cells where they appear to be retained. C LPS treatment leads to nitrosylation of both Cathepsin B and the 26S proteasomal subunits resulting in impairment of the autophagy and proteasomal degradation pathways. The increased EV packaging of these nitrosylated proteins may be an attempt by the cells to restore protein degradation pathways through removal of these impaired proteins. D Increased nitrosylation of Cofilin-1, as a result of LPS stimulation, enables the protein to sever actin filaments releasing actin, which also undergoes nitrosylation, for cytoskeletal remodelling. This allows microglia to undergo the structural changes required to achieve their activated state. The nitrosylated form of integrin α-5 (ITGA5), a protein known to interact with actin and undergo nitrosylation, was found to have reduced EV packaging implying it may be retained in the cells.

more, NAMPT transported in EVs from microglia enhances nicotinamide adenine dinucleotide (NAD) synthesis in recipient cells, a known anti-inflammatory and antioxidant molecule (Carotti et al., 2022; Yoshida et al., 2019). Together these results are consistent with LPS stimulation and show the immune response extends into the selective packaging of the released EVs.

The impact inflammation has on EV biogenesis and secretion was supported by the detection of differentially S-nitrosylated Rab proteins known to be involved in EV biogenesis. Decreased S-nitrosylation of Ras-related protein Rab-14 relative to its total proteome was observed in the LPS treated microglial derived EVs. Rab-14 is known to regulate EV secretion through regulation of late endosomes and reduced S-nitrosylation at position C26, a GTP binding domain, may indicate GTP occupancy and therefore

active Rab recruitment of vesicular cargo (Linnemannstöns et al., 2022). Further evidence for LPS stimulation affecting EV cargo loading can be observed in a previously published paper by Qu et al. (2014) which used serum starved BV-2 microglial cells treated with LPS for 16 h before undergoing iodolabelling using the iodoTMTsixplex™ Isobaric Mass Tagging Kit (ThermoFisher Scientific) (Qu et al., 2014). The use of a cell culture microglial line, serum free conditions, a relatively long LPS exposure, and an identical iodolabelling kit allowed for comparison with the results of our current study (Table S1) (Qu et al., 2014). Qu et al. (2014), observed increased S-nitrosylation of heterogenous nuclear riboproteins which are known to be involved in RNA cargo loading of EVs (Fabbiano et al., 2020). Interestingly, the S-nitrosylated cysteine is located at position C99 which falls within the 69–154 region pertaining to the protein's RNA recognition motif (Qu et al., 2014). Both the 40S ribosomal protein SA and Cofilin-1 were observed to have increased S-nitrosylation relative to their total proteome in the LPS-treated microglial EVs and were observed to exhibit increased S-nitrosylation in the LPS treated microglial cells (Qu et al., 2014). S-nitrosylation of Cofilin-1, an actin binding protein, has been observed in endothelial cells where the NO-modification enhanced Cofilin-1 activity, allowing it to mediate actin severing, cytoskeletal remodelling and migration (Zhang et al., 2011; Zhang, Lechuga et al., 2015; Zhang, Wang et al., 2015). Furthermore, actin S-nitrosylation is known to occur under inflammatory conditions, which further contributes to cytoskeleton remodelling (Lu et al., 2011; Ronzier et al., 2022). Interestingly, Qu et al., 2014 saw increased S-nitrosylation in actin, which was observed in our study where increased actin S-nitrosylation and protein expression was detected in the LPS-treated microglial EVs (Qu et al., 2014). Conversely, whilst PKM, α-enolase, and T-complex protein 1 subunit gamma were determined to have decreased S-nitrosylation relative to their total proteome in the LPS-treated microglial EVs, these proteins were found to have increased S-nitrosylation in the LPS treated microglial cells (Qu et al., 2014). α-enolase and PKM both play vital roles in glycolysis, a process that is altered in LPS stimulated macrophages (Yu et al., 2020). Specifically, LPS-treated macrophages rely on glycolysis and the tricarboxylic acid cycle to accumulate itaconate and succinate leading to Hypoxia Inducible Factor 1α stabilization and further glycolytic gene transcription, perpetuating the metabolic pathway (Viola et al., 2019). NO-modification of α-enolase is known to impair this pathway in diabetic cardiomyopathy (Lu et al., 2010, 2014). Therefore, the retention of S-nitrosylated α-enolase in the cells may be indicative of impaired glycolytic activity, a function that has been observed in neurodegenerative diseases including Alzheimer's disease where reduced brain glucose metabolism is an early sign of the disease (Castegna et al., 2002; Duran-Aniotz & Hetz, 2016; Kuehn, 2020). Both studies detected differential S-nitrosylation of lactase dehydrogenase members and tubulin chains (Qu et al., 2014). This comparison has provided a greater understanding into how the protein modifications detected in our study may be packaged into EVs and sheds insight on their contribution to aspects of EV biogenesis and cargo loading.

Finally, STRING analysis demonstrated interconnectivity and complex network relationships between differentially S-nitrosylated EV proteins, which was not observed when examining the total proteome alone. Therefore, it appears that S-nitrosylation changes have a greater impact on pathways and interactions between proteins being selectively packaged into EVs during neuroinflammation than just differential expression alone. This is particularly important as protein interaction networks likely have a summative effect on overall EV function, with the results observed here broadly indicating alterations in proteostasis and immunomodulation pathways in a more meaningful way than our interrogation of differential expression alone. Notably, protein S-nitrosylation has previously been shown to compete with other protein modifications, particularly lipidations, which play a role in regulating endo-membrane localisation (Robinson et al., 2018). This raises the possibility that NO-modifications could act as an independent regulator of EV cargo loading via restricting proteins to the cytosolic space. Recently, a lipidated ESCRT-III construct was found to be capable of generating ILVs (Marklew et al., 2018). This coupled with the lipidation of proteins involved in EV biogenesis and generation suggests that NO-modifications may have implications for EV formation and maturation affecting the vesicles released (Kwiatkowska et al., 2020; Marklew et al., 2018). Finally, given the NO-modification of several transmembrane proteins discovered in this study, including macrosialin and monocyte differentiation antigen CD14, the effects of this inflammatory induced modification may extend to EV function in the form of uptake and cellular communication as the status of these proteins as microglial markers (Jurga et al., 2020). Future studies will be required to elucidate the importance of protein NO-modification on these processes, particularly EV biogenesis and cellular uptake, where NO could act as a local inflammatory signal modulating EV physiology at a fundamental level.

In conclusion, neuroinflammation elicited by LPS treatment activates microglial expression of the gene Nos2, resulting in iNOS expression and allowing for the generation of NO which exerts its effects through 3-nitrotyrosine formation and the S-nitrosylation of target thiols on cysteines. This study has revealed that EVs released from LPS-treated microglia exhibit NO-modified protein cysteine thiol side chains using novel surface imaging. Furthermore, this study demonstrated through iodolabelling and proteomic analysis that these changes lead to protein S-nitrosylation patterns indicative of neuroinflammation, with a large proportion of NO-modified proteins being functionally involved in immunomodulation. Together, these results show activation of microglia results in broad signalling changes extending into the selective packaging of EVs and more generally highlights the importance of protein post-translational modifications in EV communication during neuroinflammation.

AUTHOR CONTRIBUTIONS

Natasha Vassileff: Conceptualization (equal); formal analysis (equal); methodology (equal); writing—original draft (equal). **Jereme G. Spiers**: Conceptualization (equal); formal analysis (equal); investigation (equal); writing—original draft (equal). **Sarah**

E. Bamford: Conceptualization (equal); formal analysis (equal); investigation (equal); writing—original draft (equal). **Rohan G. T. Lowe**: Formal analysis (equal); writing—review and editing (equal). **Keshava K. Datta**: Formal analysis (equal); writing—review and editing (equal). **Paul J. Pigram**: Conceptualization (equal); methodology (equal); resources (equal); supervision (equal); writing—review and editing (equal). **Andrew F. Hill**: Conceptualization (equal); methodology (equal); resources (equal); supervision (equal); writing—review and editing (equal).

CONFLICT OF INTEREST STATEMENT

The authors declare no conflicts of interest.

DATA AVAILABILITY STATEMENT

All data is included in the manuscript or supplemental figures. Primary images are available upon request.

ORCID

Natasha Vassileff https://orcid.org/0000-0001-6554-4496
Jereme G. Spiers https://orcid.org/0000-0001-5872-8983
Paul J. Pigram https://orcid.org/0000-0002-7972-492X
Andrew F. Hill https://orcid.org/0000-0001-5581-2354

REFERENCES

Bamford, S. E., Vassileff, N., Spiers, J. G., Gardner, W., Winkler, D. A., Muir, B. W., Hill, A. F., & Pigram, P. J. (2023). High resolution imaging and analysis of extracellular vesicles using mass spectral imaging and machine learning. *Journal of Extracellular Biology*, 2, e110.

Bell-Temin, H., Culver-Cochran, A. E., Chaput, D., Carlson, C. M., Kuehl, M., Burkhardt, B. R., Bickford, P. C., Liu, B., & Stevens, S. M. Jr. (2015). Novel molecular insights into classical and alternative activation states of microglia as revealed by stable isotope labeling by amino acids in cell culture (SILAC)-based proteomics. *Molecular & Cellular Proteomics*, 14, 3173–3184.

Bochmann, I., Ebstein, F., Lehmann, A., Wohlschlaeger, J., Sixt, S. U., Kloetzel, P. M., & Dahlmann, B. (2014). T lymphocytes export proteasomes by way of microparticles: A possible mechanism for generation of extracellular proteasomes. *Journal of Cellular and Molecular Medicine*, 18, 59–68.

Bolte, S., & CordeliÈRes, F. P. (2006). A guided tour into subcellular colocalization analysis in light microscopy. *Journal of Microscopy*, 224, 213–232.

Bourgognon, J. M., Spiers, J. G., Robinson, S. W., Scheiblich, H., Glynn, P., Ortori, C., Bradley, S. J., Tobin, A. B., & Steinert, J. R. (2021). Inhibition of neuroinflammatory nitric oxide signaling suppresses glycation and prevents neuronal dysfunction in mouse prion disease. *PNAS*, 118, e2009579118.

Carotti, V., van der Wijst, J., Verschuren, E. H. J., Rutten, L., Sommerdijk, N., Kaffa, C., Sommers, V., Rigalli, J. P., & Hoenderop, J. G. J. (2022). Involvement of ceramide biosynthesis in increased extracellular vesicle release in Pkd1 knock out cells. *Front Endocrinol (Lausanne)*, 13, 1005639.

Castegna, A., Aksenov, M., Thongboonkerd, V., Klein, J. B., Pierce, W. M., Booze, R., Markesbery, W. R., & Butterfield, D. A. (2002). Proteomic identification of oxidatively modified proteins in Alzheimer's disease brain. Part II: dihydropyrimidinase-related protein 2, alpha-enolase and heat shock cognate 71. *Journal of Neurochemistry*, 82, 1524–1532.

Chen, H.-J. C., Lee, J. K., Yip, T., Sernia, C., Lavidis, N. A., & Spiers, J. G. (2019). Sub-acute restraint stress progressively increases oxidative/nitrosative stress and inflammatory markers while transiently upregulating antioxidant gene expression in the rat hippocampus. *Free Radical Biology and Medicine*, 130, 446–457.

Chiaradia, E., Tancini, B., Emiliani, C., Delo, F., Pellegrino, R. M., Tognoloni, A., Urbanelli, L., & Buratta, S. (2021). Extracellular vesicles under oxidative stress conditions: Biological properties and physiological roles. *Cells*, 10(7), 1763.

Duran-Aniotz, C., & Hetz, C. (2016). Glucose Metabolism: A Sweet Relief of Alzheimer's Disease. *Current biology: CB*, 26(17), R806–R809.

Ebrahimi, K. B., Fijalkowski, N., Cano, M., & Handa, J. T. (2013). Decreased membrane complement regulators in the retinal pigmented epithelium contributes to age-related macular degeneration. *Journal of Pathology*, 229, 729–742.

Eitan, E., Suire, C., Zhang, S., & Mattson, M. P. (2016). Impact of lysosome status on extracellular vesicle content and release. *Ageing Research Reviews*, 32, 65–74.

Fabbiano, F., Corsi, J., Gurrieri, E., Trevisan, C., Notarangelo, M., & D'Agostino, V. G. (2020). RNA packaging into extracellular vesicles: An orchestra of RNA-binding proteins? *Journal of Extracellular Vesicles*, 10, e12043.

Fonseka, P., Pathan, M., Chitti, S. V., Kang, T., & Mathivanan, S. (2021). FunRich enables enrichment analysis of OMICs datasets. *Journal of Molecular Biology*, 433, 166747.

Futami, Y., Takeda, Y., Koba, T., Narumi, R., Nojima, Y., Ito, M., Nakayama, M., Ishida, M., Yoshimura, H., Naito, Y., Fukushima, K., Takimoto, T., Edahiro, R., Matsuki, T., Nojima, S., Hirata, H., Koyama, S., Iwahori, K., Nagatomo, I., … Kumanogoh, A. (2022). Identification of CD14 and lipopolysaccharide-binding protein as novel biomarkers for sarcoidosis using proteomics of serum extracellular vesicles. *International Immunology*, *34*, 327–340.

Galea, E., Feinstein, D. L., & Reis, D. J. (1992). Induction of calcium-independent nitric oxide synthase activity in primary rat glial cultures. *PNAS*, *89*, 10945–10949.

Hassani, K., & Olivier, M. (2013). Immunomodulatory impact of leishmania-induced macrophage exosomes: A comparative proteomic and functional analysis. *PLoS Neglected Tropical Diseases*, *7*, e2185.

Hughes, C. S., Moggridge, S., Müller, T., Sorensen, P. H., Morin, G. B., & Krijgsveld, J. (2019). Single-pot, solid-phase-enhanced sample preparation for proteomics experiments. *Nature Protocols*, *14*, 68–85.

Iizumi, T., Takahashi, S., Mashima, K., Minami, K., Izawa, Y., Abe, T., Hishiki, T., Suematsu, M., Kajimura, M., & Suzuki, N. (2016). A possible role of microglia-derived nitric oxide by lipopolysaccharide in activation of astroglial pentose-phosphate pathway via the Keap1/Nrf2 system. *Journal of Neuroinflammation*, *13*, 99.

Javeed, N., Her, T. K., Brown, M. R., Vanderboom, P., Rakshit, K., Egan, A. M., Vella, A., Lanza, I., & Matveyenko, A. V. (2021). Pro-inflammatory β cell small extracellular vesicles induce β cell failure through activation of the CXCL10/CXCR3 axis in diabetes. *Cell Reports*, *36*, 109613.

Jurga, A. M., Paleczna, M., & Kuter, K. Z. (2020). Overview of general and discriminating markers of differential microglia phenotypes. *Frontiers in Cellular Neuroscience*, *14*, 198.

Kapadia, M. R., Eng, J. W., Jiang, Q., Stoyanovsky, D. A., & Kibbe, M. R. (2009). Nitric oxide regulates the 26S proteasome in vascular smooth muscle cells. *Nitric Oxide*, *20*, 279–288.

Karampela, I., Christodoulatos, G. S., Kandri, E., Antonakos, G., Vogiatzakis, E., Dimopoulos, G., Armaganidis, A., & Dalamaga, M. (2019). Circulating eNampt and resistin as a proinflammatory duet predicting independently mortality in critically ill patients with sepsis: A prospective observational study. *Cytokine*, *119*, 62–70.

Kim, K.-R., Cho, E.-J., Eom, J.-W., Oh, S.-S., Nakamura, T., Oh, C. K., Lipton, S. A., & Kim, Y.-H. (2022). S-Nitrosylation of cathepsin B affects autophagic flux and accumulation of protein aggregates in neurodegenerative disorders. *Cell Death & Differentiation*, *29*, 2137–2150.

Kuehn, B. M. (2020). In Alzheimer research, glucose metabolism moves to center stage. *Jama*, *323*, 297–299.

Kumar, A., Chen, S. H., Kadiiska, M. B., Hong, J. S., Zielonka, J., Kalyanaraman, B., & Mason, R. P. (2014). Inducible nitric oxide synthase is key to peroxynitrite-mediated, LPS-induced protein radical formation in murine microglial BV2 cells. *Free Radical Biology and Medicine*, *73*, 51–59.

Kwiatkowska, K., Matveichuk, O. V., Fronk, J., & Ciesielska, A. (2020). Flotillins: At the intersection of protein S-palmitoylation and lipid-mediated signaling. *International Journal of Molecular Sciences*, *21*, 2283.

Li, J., Baud, O., Vartanian, T., Volpe, J. J., & Rosenberg, P. A. (2005). Peroxynitrite generated by inducible nitric oxide synthase and NADPH oxidase mediates microglial toxicity to oligodendrocytes. *PNAS*, *102*, 9936–9941.

Linnemannstöns, K., Karuna, M. P., Witte, L., Choezom, D., Honemann-Capito, M., Lagurin, A. S., Schmidt, C. V., Shrikhande, S., Steinmetz, L. K., Wiebke, M., Lenz, C., & Gross, J. C. (2022). Microscopic and biochemical monitoring of endosomal trafficking and extracellular vesicle secretion in an endogenous in vivo model. *Journal of Extracellular Vesicles*, *11*, e12263.

Lu, J., Katano, T., Uta, D., Furue, H., & Ito, S. (2011). Rapid S-nitrosylation of actin by NO-generating donors and in inflammatory pain model mice. *Molecular Pain*, *7*, 101.

Lu, N., Zhang, Y., Li, H., & Gao, Z. (2010). Oxidative and nitrative modifications of α-enolase in cardiac proteins from diabetic rats. *Free Radical Biology and Medicine*, *48*, 873–881.

Lu, N., Li, J., He, Y., Tian, R., & Xiao, Q. (2014). Nitrative modifications of α-enolase in hepatic proteins from diabetic rats: The involvement of myeloperoxidase. *Chemico-Biological Interactions*, *220*, 12–19.

Mahida, R. Y., Price, J., Lugg, S. T., Li, H., Parekh, D., Scott, A., Harrison, P., Matthay, M. A., & Thickett, D. R. (2022). CD14-positive extracellular vesicles in bronchoalveolar lavage fluid as a new biomarker of acute respiratory distress syndrome. *American Journal of Physiology. Lung Cellular and Molecular Physiology*, *322*, L617–l624.

Marklew, C. J., Booth, A., Beales, P. A., & Ciani, B. (2018). Membrane remodelling by a lipidated endosomal sorting complex required for transport-III chimera, in vitro. *Interface Focus*, *8*, 20180035.

Mizushima, N. (2007). Autophagy: Process and function. *Genes & Development*, *21*, 2861–2873.

Murray, C. I., Uhrigshardt, H., O'Meally, R. N., Cole, R. N., & Van Eyk, J. E. (2012). Identification and quantification of S-nitrosylation by cysteine reactive tandem mass tag switch assay. *Molecular & Cellular Proteomics*, *11*, M111.013441.

Murrow, L., Malhotra, R., & Debnath, J. (2015). ATG12-ATG3 interacts with Alix to promote basal autophagic flux and late endosome function. *Nature Cell Biology*, *17*, 300–310.

Nakamura, T., & Lipton, S. A. (2019). Nitric oxide-dependent protein post-translational modifications impair mitochondrial function and metabolism to contribute to neurodegenerative diseases. *Antioxidants & Redox Signaling*, *32*, 817–833.

Papageorgiou, I. E., Lewen, A., Galow, L. V., Cesetti, T., Scheffel, J., Regen, T., Hanisch, U. K., & Kann, O. (2016). TLR4-activated microglia require IFN-γ to induce severe neuronal dysfunction and death in situ. *Proceedings of the National Academy of Sciences of the United States of America*, *113*, 212–217.

Prebanda, M., Završnik, T., & Kopitar-Jerala, N. (2019). Upregulation of mitochondrial redox sensitive proteins in LPS-treated stefin B-deficient macrophages. *Cells*, *8*, 1476.

Qu, Z., Meng, F., Bomgarden, R. D., Viner, R. I., Li, J., Rogers, J. C., Cheng, J., Greenlief, C. M., Cui, J., Lubahn, D. B., Sun, G. Y., & Gu, Z. (2014). Proteomic quantification and site-mapping of S-nitrosylated proteins using isobaric iodoTMT reagents. *Journal of Proteome Research*, *13*, 3200–3211.

Rappsilber, J., Mann, M., & Ishihama, Y. (2007). Protocol for micro-purification, enrichment, pre-fractionation and storage of peptides for proteomics using StageTips. *Nature Protocols*, *2*, 1896–1906.

Real, J. M., Ferreira, L. R. P., Esteves, G. H., Koyama, F. C., Dias, M. V. S., Bezerra-Neto, J. E., Cunha-Neto, E., Machado, F. R., Salomão, R., & Azevedo, L. C. P. (2018). Exosomes from patients with septic shock convey miRNAs related to inflammation and cell cycle regulation: New signaling pathways in sepsis? *Critical Care (London, England)*, *22*, 68.

Robinson, S. W., Bourgognon, J.-M., Spiers, J. G., Breda, C., Campesan, S., Butcher, A., Mallucci, G. R., Dinsdale, D., Morone, N., Mistry, R., Smith, T. M., Guerra-Martin, M., Challiss, R. A. J., Giorgini, F., & Steinert, J. R. (2018). Nitric oxide-mediated posttranslational modifications control neurotransmitter release by modulating complexin farnesylation and enhancing its clamping ability. *PLoS Biology*, *16*, e2003611.

Ronzier, E., Laurenson, A. J., Manickam, R., Liu, S., Saintilma, I. M., Schrock, D. C., Hammer, J. A., & Rotty, J. D. (2022). The actin cytoskeleton responds to inflammatory cues and alters macrophage activation. *Cells*, *11*(11), 1806.

Seth, P., Hsieh, P. N., Jamal, S., Wang, L., Gygi, S. P., Jain, M. K., Coller, J., & Stamler, J. S. (2019). Regulation of microRNA machinery and development by interspecies S-nitrosylation. *Cell*, *176*, 1014–1025. e1012.

Spiers, J. G., Vassileff, N., & Hill, A. F. (2022). Neuroinflammatory modulation of extracellular vesicle biogenesis and cargo loading. *Neuromolecular Medicine*, *24*, 385–391.

Spiers, J. G., Chen, H. C., Bourgognon, J. M., & Steinert, J. R. (2019). Dysregulation of stress systems and nitric oxide signaling underlies neuronal dysfunction in Alzheimer's disease. *Free Radical Biology and Medicine*, *134*, 468–483.

Szklarczyk, D., Franceschini, A., Wyder, S., Forslund, K., Heller, D., Huerta-Cepas, J., Simonovic, M., Roth, A., Santos, A., Tsafou, K. P., Kuhn, M., Bork, P., Jensen, L. J., & von Mering, C. (2015). STRING v10: Protein-protein interaction networks, integrated over the tree of life. *Nucleic Acids Research*, *43*, D447–452.

Tan, J., Zhang, J., Wang, M., Wang, Y., Dong, M., Ma, X., Sun, B., Liu, S., Zhao, Z., Chen, L., Jin, W., Liu, K., Xin, Y., & Zhuang, L. (2022). DRAM1 increases the secretion of PKM2-enriched EVs from hepatocytes to promote macrophage activation and disease progression in ALD. *Molecular Therapy Nucleic Acids*, *27*, 375–389.

Théry, C., Witwer, K. W., Aikawa, E., Alcaraz, M. J., Anderson, J. D., Andriantsitohaina, R., Antoniou, A., Arab, T., Archer, F., Atkin-Smith, G. K., Ayre, D. C., Bach, J. M., Bachurski, D., Baharvand, H., Balaj, L., Baldacchino, S., Bauer, N. N., Baxter, A. A., Bebawy, M., … Zuba-Surma, E. K. (2018). Minimal information for studies of extracellular vesicles 2018 (MISEV2018): A position statement of the International Society for Extracellular Vesicles and update of the MISEV2014 guidelines. *Journal of Extracellular Vesicles*, *7*, 1535750.

Todorova, D., Simoncini, S., Lacroix, R., Sabatier, F., & Dignat-George, F. (2017). Extracellular vesicles in angiogenesis. *Circulation Research*, *120*, 1658–1673.

Viola, A., Munari, F., Sánchez-Rodríguez, R., Scolaro, T., & Castegna, A. (2019). The metabolic signature of macrophage responses. *Frontiers in Immunology*, *10*, 1462.

Wijasa, T. S., Sylvester, M., Brocke-Ahmadinejad, N., Kummer, M. P., Brosseron, F., Gieselmann, V., & Heneka, M. T. (2017). Proteome profiling of s-nitrosylated synaptosomal proteins by isobaric mass tags. *Journal of Neuroscience Methods*, *291*, 95–100.

Wijasa, T. S., Sylvester, M., Brocke-Ahmadinejad, N., Schwartz, S., Santarelli, F., Gieselmann, V., Klockgether, T., Brosseron, F., & Heneka, M. T. (2020). Quantitative proteomics of synaptosome S-nitrosylation in Alzheimer's disease. *Journal of Neurochemistry*, *152*, 710–726.

Xu, D., Li, T., Wang, R., & Mu, R. (2021). Expression and pathogenic analysis of integrin family genes in systemic sclerosis. *Frontiers in Medicine (Lausanne)*, *8*, 674523.

Yaker, L., Tebani, A., Lesueur, C., Dias, C., Jung, V., Bekri, S., Guerrera, I. C., Kamel, S., Ausseil, J., & Boullier, A. (2022). Extracellular vesicles from LPS-treated macrophages aggravate smooth muscle cell calcification by propagating inflammation and oxidative stress. *Frontiers in Cell and Developmental Biology*, *10*, 823450.

Yang, H., Zhu, Y., Ye, Y., Guan, J., Min, X., & Xiong, H. (2022). Nitric oxide protects against cochlear hair cell damage and noise-induced hearing loss through glucose metabolic reprogramming. *Free Radical Biology Medicine*, *179*, 229–241.

Yang, Y., Boza-Serrano, A., Dunning, C. J. R., Clausen, B. H., Lambertsen, K. L., & Deierborg, T. (2018). Inflammation leads to distinct populations of extracellular vesicles from microglia. *Journal of Neuroinflammation*, *15*, 168.

Yoshida, M., Satoh, A., Lin, J. B., Mills, K. F., Sasaki, Y., Rensing, N., Wong, M., Apte, R. S., & Imai, S. I. (2019). Extracellular vesicle-contained eNAMPT delays aging and extends lifespan in mice. *Cell Metabolism*, *30*, 329–342. e325.

Yu, Q., Wang, Y., Dong, L., He, Y., Liu, R., Yang, Q., Cao, Y., Wang, Y., Jia, A., Bi, Y., & Liu, G. (2020). Regulations of glycolytic activities on macrophages functions in tumor and infectious inflammation. *Frontiers in Cellular and Infection Microbiology*, *10*, 287.

Zhang, H. H., Hachey, S., Feng, L., Wang, W., Satohisa, S., & Chen, D. B. (2011). S-Nitrosylation of cofilin-1 is a novel pathway for endothelial cell migration. *Biology of Reproduction*, *85*, 64–64.

Zhang, H. H., Lechuga, T. J., Tith, T., Wang, W., Wing, D. A., & Chen, D. B. (2015). S-Nitrosylation of cofilin-1 mediates estradiol-17β-stimulated endothelial cytoskeleton remodeling. *Molecular Endocrinology*, *29*, 434–444.

Zhang, H., Zhang, S. J., Lyn, N., Florentino, A., Li, A., Davies, K. J. A., & Forman, H. J. (2020). Down regulation of glutathione and glutamate cysteine ligase in the inflammatory response of macrophages. *Free Radical Biology Medicine*, *158*, 53–59.

Zhang, H. H., Wang, W., Feng, L., Yang, Y., Zheng, J., Huang, L., & Chen, D. B. (2015). S-nitrosylation of cofilin-1 serves as a novel pathway for VEGF-stimulated endothelial cell migration. *Journal of Cellular Physiology*, *230*, 406–417.

Zhao, W., Spiers, J. G., Vassileff, N., Khadka, A., Jaehne, E. J., van den Buuse, M., & Hill, A. F. (2023). MicroRNA-146a modulates behavioural activity, neuroinflammation, and oxidative stress in adult mice. *Molecular and Cellular Neuroscience*, *124*, 103820.

SUPPORTING INFORMATION

Additional supporting information can be found online in the Supporting Information section at the end of this article.

How to cite this article: Vassileff, N., Spiers, J. G., Bamford, S. E., Lowe, R. G. T., Datta, K. K., Pigram, P. J., & Hill, A. F. (2024). Microglial activation induces nitric oxide signalling and alters protein S-nitrosylation patterns in extracellular vesicles. *Journal of Extracellular Vesicles*, *13*, e12455. https://doi.org/10.1002/jev2.12455